

CONSTRAINING DARK MATTER HALO PROFILES AND GALAXY FORMATION MODELS USING SPIRAL ARM MORPHOLOGY. II. DARK AND STELLAR MASS CONCENTRATIONS FOR 13 NEARBY FACE-ON GALAXIES

MARC S. SEIGAR^{1,2}, BENJAMIN L. DAVIS³, JOEL BERRIER^{3,4,5}, AND DANIEL KENNEFICK^{3,4}

Draft version January 8, 2018

ABSTRACT

We investigate the use of spiral arm pitch angles as a probe of disk galaxy mass profiles. We confirm our previous result that spiral arm pitch angles (P) are well correlated with the rate of shear (S) in disk galaxy rotation curves. We use this correlation to argue that imaging data alone can provide a powerful probe of galactic mass distributions out to large look-back times. We then use a sample of 13 galaxies, with *Spitzer* 3.6- μm imaging data and observed H α rotation curves, to demonstrate how an inferred shear rate coupled with a bulge-disk decomposition model and a Tully-Fisher-derived velocity normalization can be used to place constraints on a galaxy's baryon fraction and dark matter halo profile. Finally we show that there appears to be a trend (albeit a weak correlation) between spiral arm pitch angle and halo concentration. We discuss implications for the suggested link between supermassive black hole (SMBH) mass and dark halo concentration, using pitch angle as a proxy for SMBH mass.

Subject headings: dark matter — galaxies: fundamental parameters — galaxies: halos — galaxies: kinematics and dynamics — galaxies: spiral — galaxies: structure

1. INTRODUCTION

The discovery of a correlation between spiral arm pitch angle and rotation curve rate of shear (Seigar, Block & Puerari 2004, Seigar et al. 2005, 2006) may be a fundamental property of galaxies that is a key in understanding mass distributions. This is because the rate of shear is related to the slope of the outer part of the rotation curve, which in turn is related to the galaxy mass distribution. In other words, shear is strongly connected to the central mass concentrations of galaxies.

The shear, S , is a dimensionless quantity, and can be measured directly from rotation curves, if one is available. It is defined as follows,

$$S = \frac{A}{\omega} = \frac{1}{2} \left(1 - \frac{R}{V} \frac{dV}{dR} \right), \quad (1)$$

where A is the first Oort constant, ω is the angular velocity and V is the velocity at a radius R . The shear rate depends upon the shape of the rotation curve. For a rotation curve that remains flat $S = 0.5$, for a falling rotation curve $S > 0.5$ and for a continually rising rotation curve $S < 0.5$. As the shape of a rotation curve depends on the mass distribution, the shear rate at any given position depends upon the mass within that radius, or the central mass concentration. As a result, the spiral arm pitch angle is dependent upon the central mass concentration, and this is consistent with the expectations

of most spiral density wave models (e.g. Bertin et al. 1989a, b; Bertin 1991, 1993, 1996; Bertin & Lin 1996; Fuchs 1991, 2000), although density wave models predict that pitch angles also depend on stability (i.e. the Toomre Q -parameter).

The correlation between shear and spiral arm pitch angles may explain the weak correlations found between properties like bulge-to-disk ratio (B/D), spiral arm pitch angle and Hubble Type (e.g. de Jong 1996; Seigar & James 1998a, b). In these studies the correlations are weak because, even the near-infrared B/D is not a complete picture when it comes to determining the central mass concentration, as the dark matter concentration is not taken into account. However, a property such as shear is sensitive to the total baryonic and dark matter concentrations.

Given the relationship between shear and spiral arm pitch angle (Seigar et al. 2006; hereafter Paper 1) it is possible to determine shear, from imaging data alone, given the equation from Paper 1,

$$P = (64.25 \pm 2.87) - (73.24 \pm 5.53)S, \quad (2)$$

where P is the pitch angle in degrees and S is the shear rate. This relationship opens up a fundamentally new approach for probing mass distributions in spiral galaxies. This approach relies on imaging data alone without the need for full rotation curve information. Specifically, the Tully-Fisher relation (Tully & Fisher 1977) for spiral galaxies coupled with the shear rate - pitch angle relation can be used to determine a rotation curve normalization *and* slope. In this paper we explicitly demonstrate how, given a bulge-disk decomposition, a pitch angle determination, and a Tully-Fisher normalization, one can constrain galaxy mass distributions, dark matter halo concentrations, and other galaxy formation parameters. We obtain our constraints within the context of the standard framework of disk formation put forth by Fall & Efstathiou (1980) and Blumenthal et al. (1986).

¹ Department of Physics, University of Minnesota Duluth, 1023 University Drive, MWAH 371, Duluth, MN 55812-3009

² Department of Physics & Astronomy, University of Arkansas at Little Rock, 2801 S. University Avenue, Little Rock, AR 72204-1099

³ Arkansas Center for Space and Planetary Sciences, 202 Field House, University of Arkansas, Fayetteville, AR 72701

⁴ Department of Physics, University of Arkansas, 835 West Dickson Street, Fayetteville, AR 72701

⁵ Department of Physics & Astronomy, Rutgers University, 136 Frelinghuysen Road, Piscataway, NJ 08854

In principle, the technique we demonstrate here and in Paper 1 can be applied generally to a large sample of galaxies and to galaxies at high redshift, when spiral arms are detected. This is the second in a series of papers in which we use spiral arm pitch angles to determine the mass distribution in spiral galaxies. In this paper we determine mass concentrations in a large sample of disk galaxies from their spiral arm pitch angles (as this is intrinsically related to their shear rates, i.e. we determine shear using equation 2), their disk masses and their disk scalelengths (determined via a bulge-disk decomposition technique).

This paper is arranged as follows. Section 2 describes the data we used and the analysis tools. Section 3 describes how we determine the stellar mass distribution in our sample of galaxies. Section 4 describes the dark matter halo density profile models we use and how we determine the halo profiles of our sample of galaxies. In section 5 we present a discussion of our results and in section 6 we provide our main conclusions and present our planned future goals.

Throughout this work we assume a Hubble constant of $h = 0.705$ in units of $100 \text{ km s}^{-1} \text{ Mpc}^{-1}$ and a cosmology with $\Omega_m = 1 - \Omega_\Lambda = 0.274$ (Komatsu et al. 2009).

2. OBSERVATIONS AND DATA REDUCTION

2.1. Data

The dataset presented in this paper consists of 13 spiral galaxies observed with *Spitzer IRAC* at $3.6\text{-}\mu\text{m}$. These galaxies were chosen as follows: a parent sample (defined as a Southern Hemisphere ($\delta < 0^\circ$) galaxies with $B_T < 12.9$) of 605 bright galaxies (Ho et al. 2011) was selected. From this sample, we then selected all galaxies with observed $\text{H}\alpha$ rotation curves from Persic & Salucci (1995) that also have *Spitzer* $3.6\text{-}\mu\text{m}$ imaging data available on the archive⁶. This results in a sample of 13 galaxies. We then measure spiral arm pitch angles, and then perform a bulge-disk decomposition, using the *Spitzer* images.

2.2. Measurement of spiral arm pitch angles

Spiral arm pitch angles are measured using the same technique employed by Davis et al. (2012). A two-dimensional fast-Fourier (2D-FFT) decomposition technique is used, which employs a program described in Schröder et al. (1994). Logarithmic spirals are assumed in the decomposition. The resulting pitch angles are listed in Table 1.

The amplitude of each Fourier component is given by

$$A(m, p) = \frac{\sum_{i=1}^I \sum_{j=1}^J I_{ij}(\ln r, \theta) \exp[-i(m\theta_p \ln r)]}{\sum_{i=1}^I \sum_{j=1}^J I_{ij}(\ln r, \theta)}, \quad (3)$$

where r and θ are polar coordinates, $I(\ln r, \theta)$ is the intensity at position $(\ln r, \theta)$, m represents the number of arms or modes, and p is the variable associated with the pitch angle P , defined by $\tan P = -(m/p)$. The resulting pitch angle measured using equation 3 is in radians, and this is later converted to degrees for ease of perception.

The images were first projected to face-on. Mean uncertainties of position angle and inclination as a function

of inclination were discussed by Considère & Athanasoula (1988). For a galaxy with low inclination, there are clearly greater uncertainties in assigning both a position angle and an accurate inclination. These uncertainties are discussed by Block et al. (1999) and Seigar et al. (2005), who take a galaxy with low inclination ($< 30^\circ$) and one with high inclination ($> 60^\circ$) and varied the inclination angle used in the correction to face-on. They found that for the galaxy with low inclination, the measured pitch angle remained the same. However, the measured pitch angle for the galaxy with high inclination varied by $\pm 10\%$. Since inclination corrections are likely to be largest for galaxies with the highest inclinations cases where inclination is $> 60^\circ$ are taken as the worst case scenario. For galaxies with inclination $i > 60^\circ$ we take into account this uncertainty. Our deprojection method assumes that spiral galaxy disks are intrinsically circular in nature.

The 2D-FFT code is then deployed to work on the deprojected images. The code requires a user-defined inner and outer radius. The outer radius is chosen as the radius at which spiral structure (on any galactic structure) can no longer be seen. The inner radius is chosen as the innermost radius which excludes any bulge and/or bar structure. While the outer radius is fairly straightforward to choose, and a slightly incorrect value will not affect the derived pitch angle, the same is not true of the inner radius. If the inner radius is chosen slightly incorrectly, the derived pitch angle can be strongly affected by (for example) an inner bar. As a result Davis et al. (2012) employed an iterative routine that chose every possible inner radius from the very central regions of the galaxy out to the user-defined outer radius. The code then outputs the pitch angle as a function of inner radius for each mode, $1 \leq m \leq 6$. For every galaxy, a range of inner radii always results in a pitch angle that remains approximately constant (Davis et al. 2012). This is the pitch angle that we chose, and the variation of the pitch angle over these radii is a measure of the error. This region is referred to as the “stable region”. Note that the 2D-FFT code actually outputs a pitch angle that is either negative or positive based upon their chirality (Davis et al. 2012). For the purpose of this paper, we report the absolute values of the pitch angle.

2.3. Measurement of shear

In this paper, 13 of the galaxies have shear values that were measured directly from their $\text{H}\alpha$ rotation curves. The shear was initially calculated in Paper 1 and the rotation curves were taken from Persic & Salucci (1995). These rotation curves are of good quality with an rms error $< 10 \text{ km s}^{-1}$, and an error associated with folding the two sides of the galaxy also $< 10 \text{ km s}^{-1}$. These rotation curves have been used to estimate the shear rates in these galaxies, using the same method used by other authors (e.g. Block et al. 1999; Seigar et al. 2005; Seigar 2005).

Using equation 1, we have calculated the shear rates for these galaxies, over the same radial ranges (i.e. the stable region) for which the pitch angles were measured. The dominant sources of error on the shear rate are the rms error in the rotation curve and the error associated with folding the two sides of the galaxy. This is typically $< 10\%$. In order to calculate the shear rate, the mean value

⁶ <http://sha.ipac.caltech.edu/applications/Spitzer/SHA/>

TABLE 1
GALAXY MEASUREMENTS

Galaxy Name	Hubble Type	b/a	V_{rec} (km s^{-1})	PA (degrees)	P (degrees)	S	L_{disk} ($\times 10^{10} L_{\odot}$)	R_d (kpc)	B/D
ESO 009-G010	SAc	0.76	2418	171	23.7±1.1	0.44±0.06	1.80±0.16	5.97±0.53	0.10±0.01
ESO 582-G012	SAc	0.60	2325	48	22.6±0.6	0.51±0.05	1.65±0.15	6.46±0.59	0.14±0.01
IC 4808	SAc	0.42	5084	45	14.1±0.4	0.63±0.02	4.71±0.45	7.52±0.72	0.06±0.01
NGC 150	SBb	0.49	1584	118	8.4±0.1	0.65±0.03	1.81±0.15	3.09±0.25	0.19±0.02
NGC 578	SABc	0.63	1628	110	18.0±0.2	0.62±0.06	1.15±0.11	6.75±0.65	0.12±0.01
NGC 908	SAc	0.43	1509	75	12.9±0.4	0.59±0.04	3.01±0.30	5.71±0.57	0.08±0.01
NGC 1292	SAc	0.43	1366	7	29.8±1.0	0.49±0.04	0.50±0.04	3.72±0.30	0.06±0.01
NGC 1300	SBbc	0.66	1577	106	31.7±1.1	0.50±0.03	2.64±0.25	9.34±0.88	0.16±0.02
NGC 1353	SABc	0.41	1525	138	36.6±1.0	0.34±0.05	2.03±0.20	4.66±0.46	0.20±0.02
NGC 1365	SBb	0.55	1636	32	35.4±1.7	0.53±0.03	6.38±0.62	9.42±0.92	0.14±0.01
NGC 1964	SABb	0.38	1659	32	13.8±0.3	0.60±0.02	1.69±0.17	6.45±0.65	0.20±0.02
NGC 3223	SABc	0.61	2891	135	10.7±2.0	0.70±0.02	6.72±0.68	9.40±0.95	0.14±0.01
NGC 3318	SABb	0.54	2775	78	36.9±6.5	0.52±0.03	2.40±0.22	6.03±0.55	0.10±0.01

NOTE. — Column (1) is galaxy name; Column (2) is galaxy Hubble type taken from de Vaucouleurs et al. (1991; hereafter RC3); Column (3) is axis ratio taken from RC3; Column (4) is the recession velocity taken from the NASA Extragalactic Database (NED); Column 5 is the Position Angle taken from RC3; Column (6) is the measured pitch angle in degrees; Column (7) is the measured shear; Column (8) is the disk luminosity determined from the bulge-disk decomposition; Column (9) is the disk scalelength determined from the bulge-disk decomposition; and Column (10) is the bulge-to-disk light ratio determined from the bulge-disk decomposition.

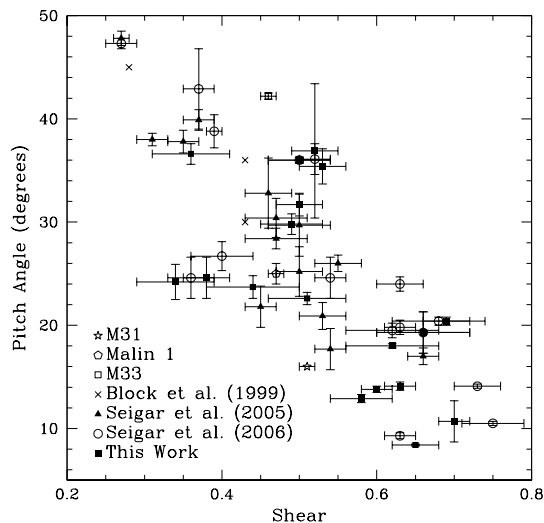


FIG. 1.— Spiral arm pitch angle vs. rotation curve shear rate, showing a correlation. The filled triangles represent galaxies with data measured by Seigar et al. (2005), the open circles are galaxies from Seigar et al. (2006), the crosses are galaxies from Block et al. (1999), the open square represents data for M33 (Seigar 2011), the open pentagon represents data for Malin 1 (Seigar 2008), the star represents data for M31 (Seigar, Barth, & Bullock 2008), and the filled squares represent the data from the present sample.

of dV/dR measured in $\text{km s}^{-1} \text{arcsec}^{-1}$ is calculated by fitting a line of constant gradient to the outer part of the rotation curve (i.e. past the radius of turnover and any bar or bulge that may exist in the galaxy) over the “stable region”, i.e., the region where the pitch angle remains approximately constant. Our measured shears are listed in Table 1.

With values for the pitch angle and shear for each galaxy, we then decided to revisit the correlation between pitch angle and shear (Seigar et al. 2005, 2006). Figure 1 shows a plot of pitch angle in degrees as a function of shear as determined above. A strong correlation still exists, although the scatter has increased a little from that

presented in Seigar et al. (2006).

3. DETERMINATION OF THE STELLAR MASS DISTRIBUTION

For each of our galaxies we produce surface brightness profiles using the IRAF **Ellipse** routine, which fits ellipses to isophotes in an image, using an iterative method described by Jedrzejewski (1987). From the surface brightness profile we then determine the disk and bulge B-band luminosity using an exponential disk and a Sérsic-law bulge. We utilize a 1-D bulge-disk decomposition routine, which performs Levenberg-Marquardt least-squares minimization. Explicitly we fit a Sérsic law profile for each bulge via

$$\mu(R) = \mu_e \exp \left\{ -b_n \left[\left(\frac{R}{R_e} \right)^{1/n} - 1 \right] \right\}, \quad (4)$$

where R_e is the effective radius, containing 50% of the total light of the bulge and μ_e is the surface brightness at R_e . The factor b_n is a function of the shape parameter, n , such that $\Gamma(2n) = 2\gamma(2n, b_n)$, where Γ is the gamma function and γ is the incomplete gamma function (see Graham & Driver 2005). As given by Capaccioli (1989), b_n can be well approximated by $1.9992n - 0.3271$ for $1 < n < 10$. In the case where $n = 1$, the Sérsic model is equivalent to an exponential, and when $n = 4$ it is equivalent to the $R^{1/4}$ model (de Vaucouleurs 1948, 1957). We fit the disk component using

$$\mu(R) = \mu_0 \exp(-R/R_d), \quad (5)$$

where μ_0 is the central surface brightness and R_d is the scalelength of the disk.

From the disk luminosity determined from the bulge-disk decomposition, we assign masses to the disk and bulge components using a range of stellar K_s -band mass-to-light ratios from Bell et al. (2003) and convert this to a $3.6\text{-}\mu\text{m}$ mass-to-light ratio using the values given for a typical disk galaxy in Seigar et al. (2008a). Specifically, in our rotation curve models we allow mass-to-light ratios of $(M/L) = 0.7, 0.8, 0.9, 1.0$ and 1.1 (measured in

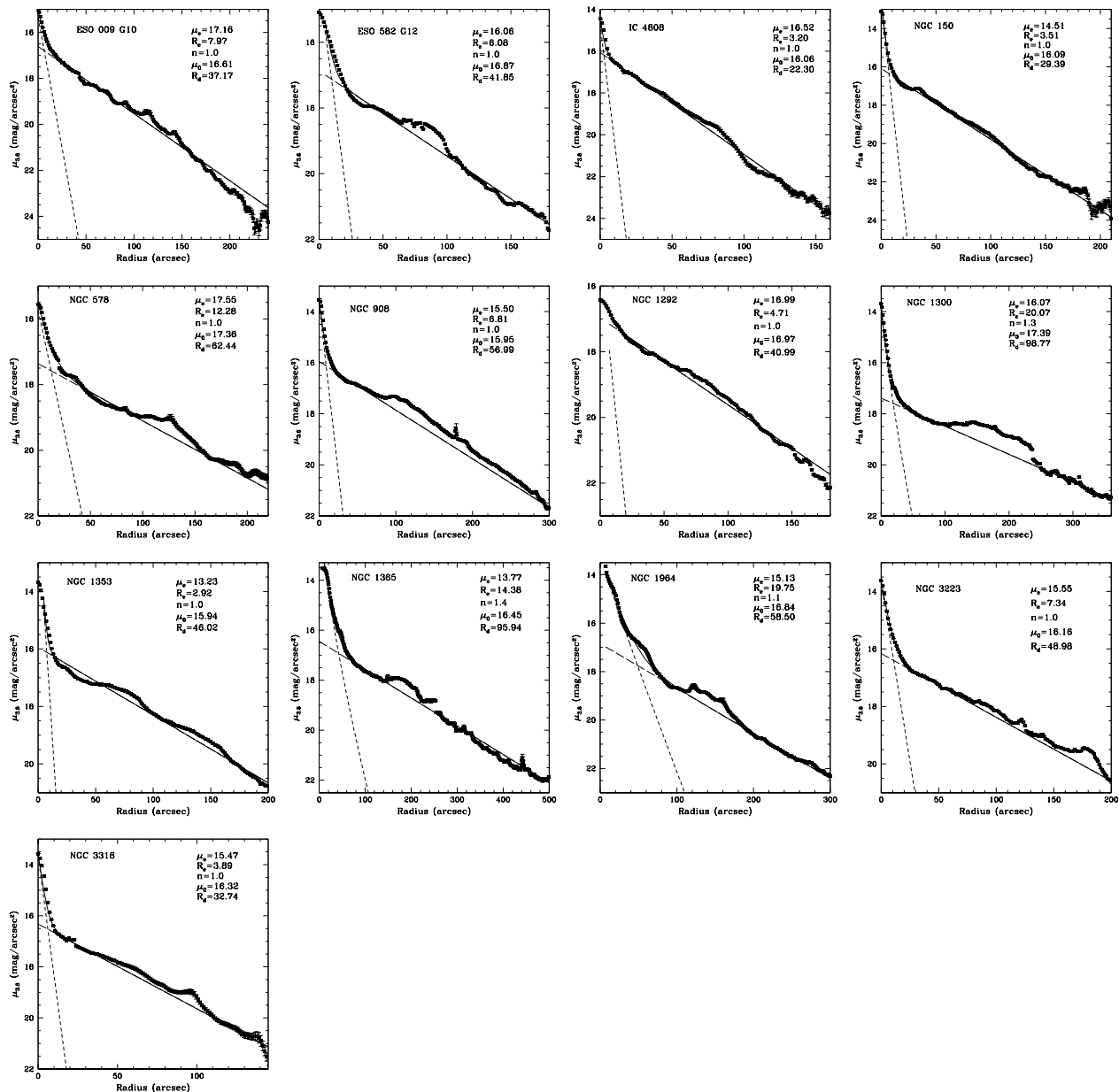


FIG. 2.— Surface brightness profiles for 13 galaxies. The short-dashed line is the Sérsic fit to the bulge, the long-dashed line is the exponential disk fit, and the solid line is the total bulge+disk fit.

3.6- μm -band solar units), and use our photometrically-derived disk and bulge light profiles $L_B = L_{\text{disk}} + L_{\text{bulge}}$ to determine the stellar mass contribution to each rotation curve: $M_* = (M/L)L_B$.

The results of our one-dimensional bulge-disk decompositions are given in Figure 2.

4. DETERMINATION OF THE DARK MATTER HALO DENSITY DISTRIBUTION

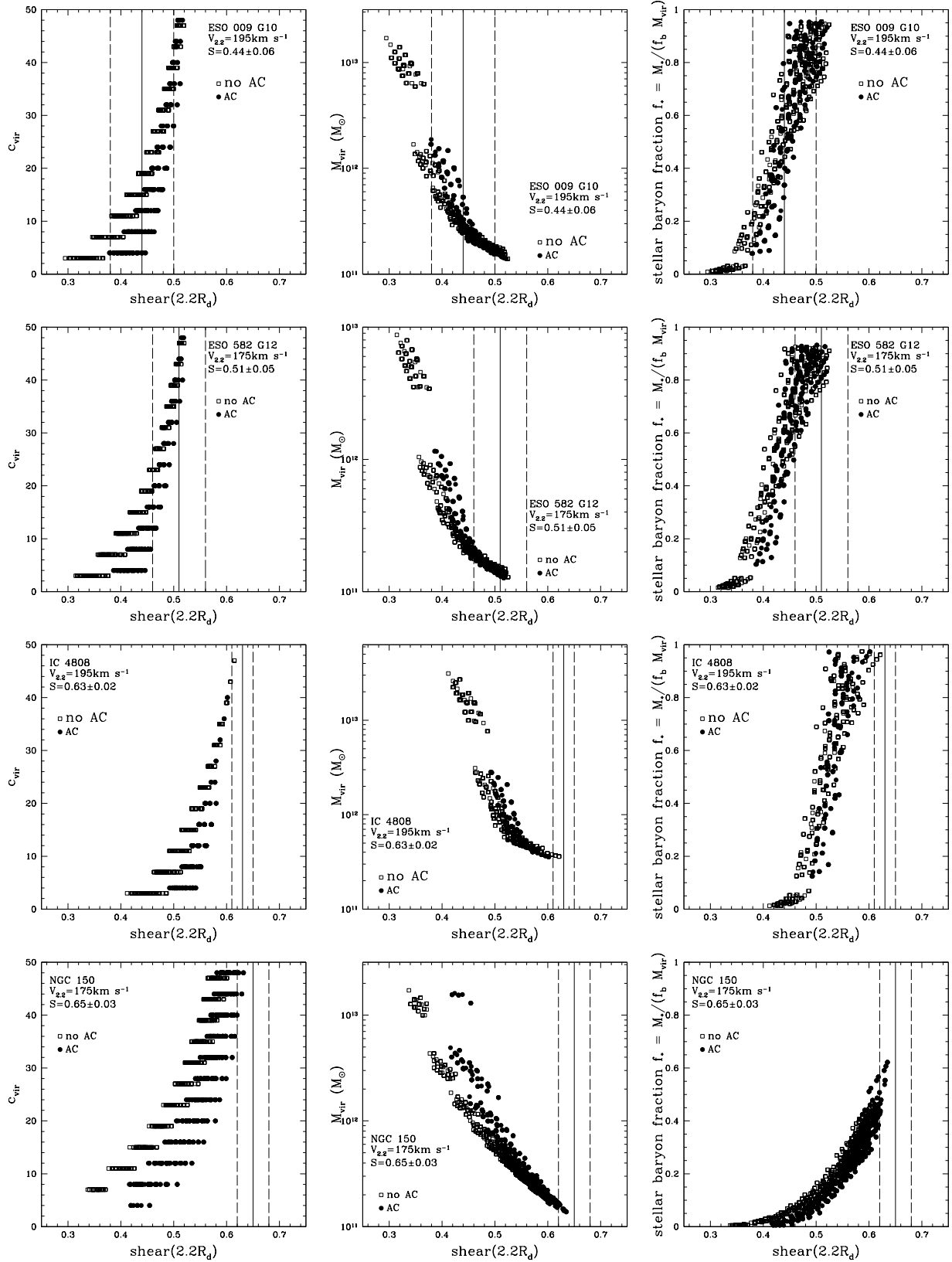
We now explore a range of allowed dark matter halo masses and density profiles by adopting two extreme models for disk galaxy formation. In the first we assume that the dark matter halos surrounding these galaxies do not undergo adiabatic contraction (AC) as a disk galaxy forms. As such, the dark matter halo density profile fol-

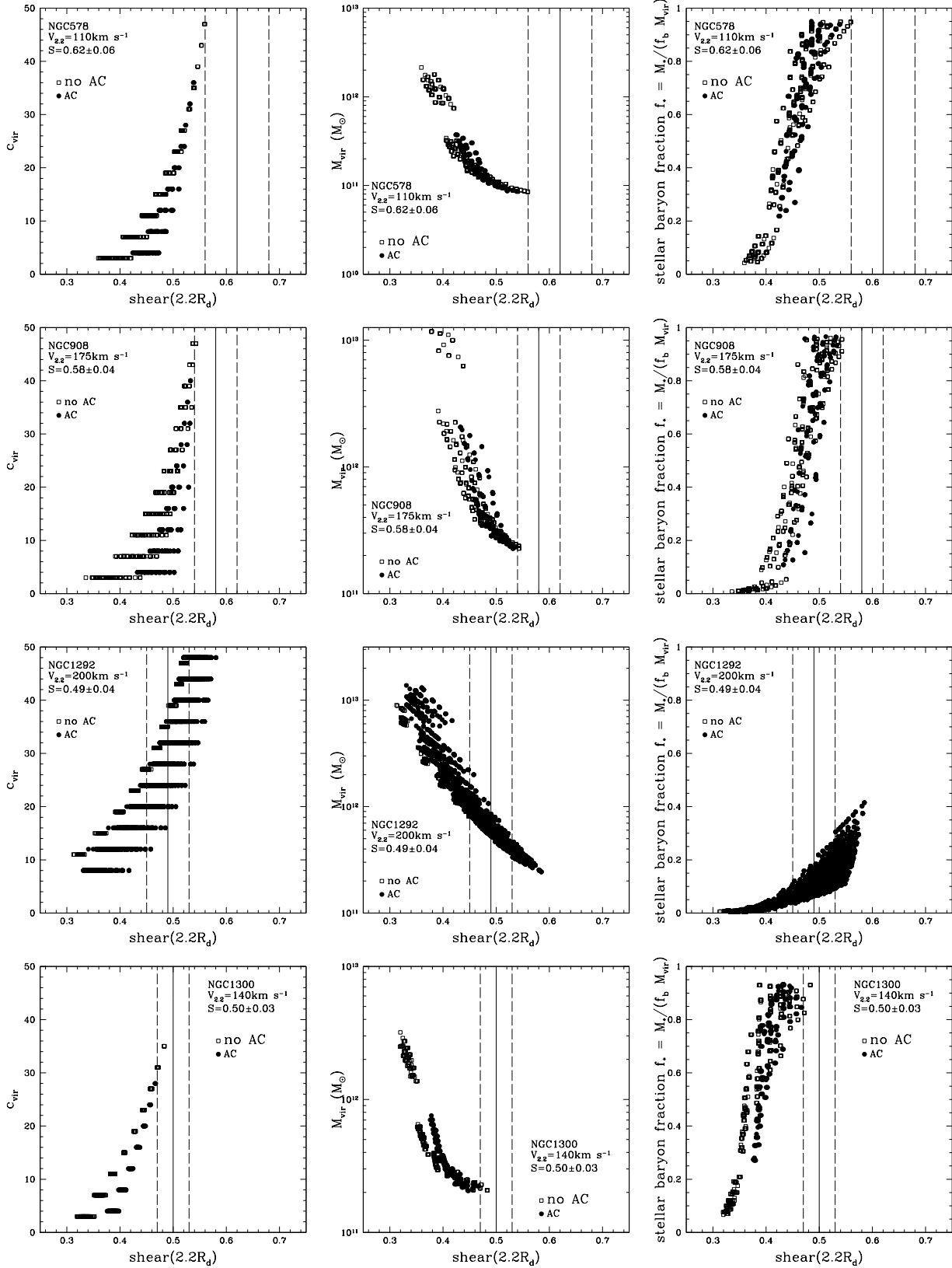
lows the following equation,

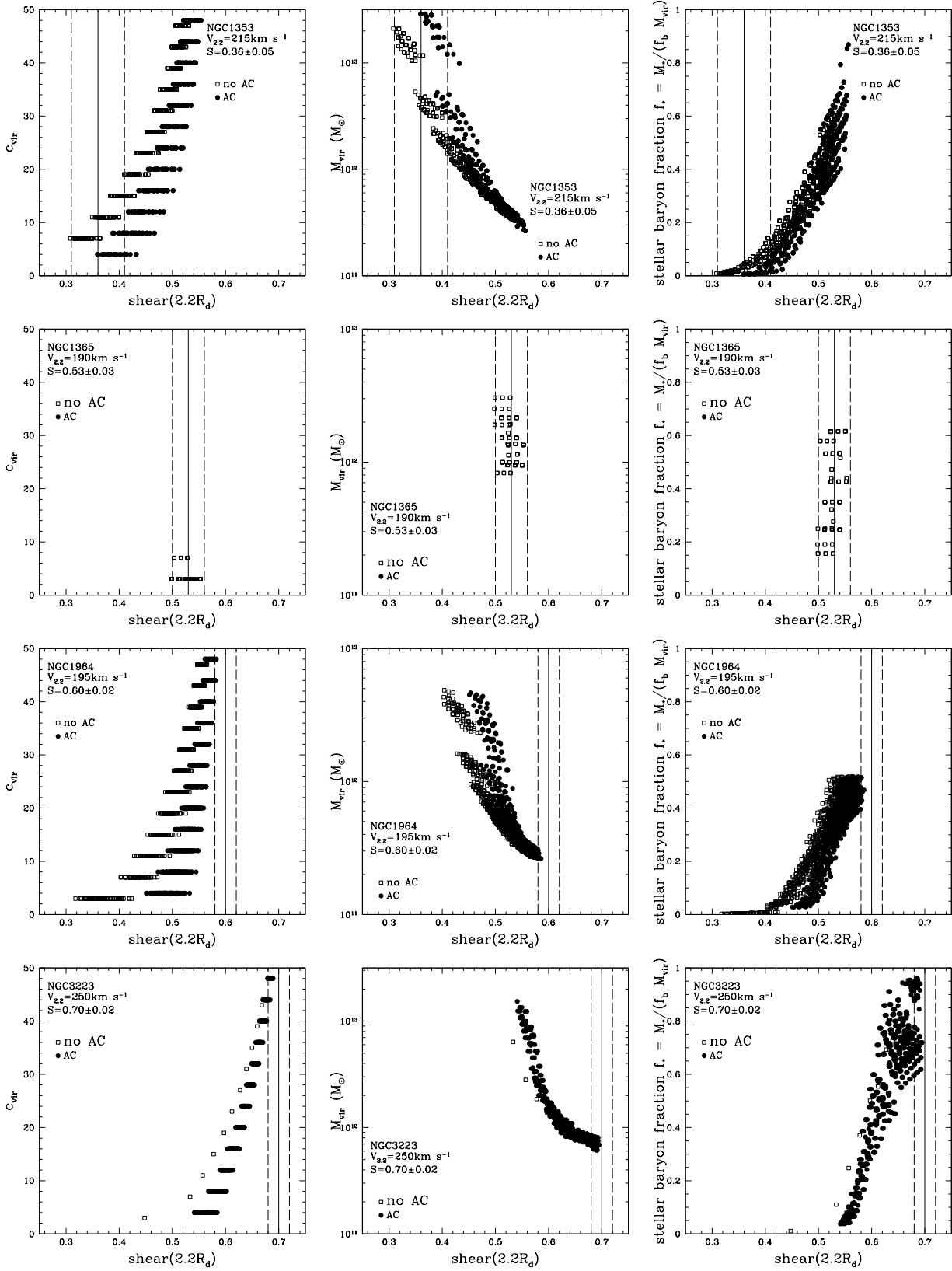
$$\rho(r) = \frac{\rho_s}{(r/r_s)(1+r/r_s)^2} \quad (6)$$

where r_s is a characteristic “inner” radius and ρ_s is the density at that radius. This is the same profile shape of Navarro et al. (1997; hereafter NFW). It is a two-parameter function, and can be completely specified by choosing two independent parameters, such as the virial mass M_{vir} and halo concentration $c_{\text{vir}} = R_{\text{vir}}/r_s$ (Bullock et al. 2001b).

For the second class of model, adiabatic contraction (AC) is adopted (Blumenthal et al. 1986; Bullock et al. 2001a; Pizagno et al. 2005). In this case the dark matter density profile initially follows an NFW profile. The baryons are then allowed to cool and settle into the halo center, and this process is much longer than one typical







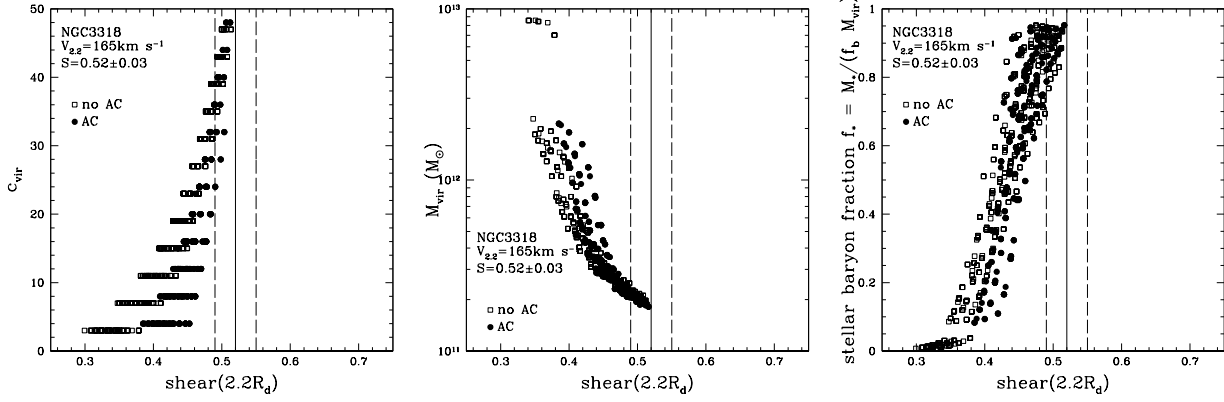


FIG. 3.— Model results for 13 galaxies. *Left*: NFW concentration vs. shear; *center*: virial mass vs. shear; *right* stellar baryon fraction vs. shear. The open squares represent the model without an adiabatically contracted dark matter halo (non-AC), and the filled circles represent the model with adiabatic contraction (AC). The vertical lines represent the measured shear (solid line) with the 1σ error added (dashed lines).

TABLE 2
GALAXY MODEL RESULTS

Galaxy Name	c_{vir}	$M_{\text{vir}} (\times 10^{12} M_{\odot})$	f_*	c_{tot}	c_{DM}
ESO 009-G010	6–42	0.05–1.05	0.10–0.95	0.02–0.30	0.02–0.18
ESO 582-G012	18–48	0.05–0.25	0.50–0.90	0.18–0.31	0.13–0.23
IC 4808	42–46	0.32–0.39	0.90–1.00	0.32–0.34	0.16–0.18
NGC 150	>48	0.14–0.29	0.38–0.47	0.34–0.42	0.26–0.28
NGC 578	40–48	0.87–0.95	0.90–0.95	0.32–0.33	0.23–0.24
NGC 908	34–48	0.21–0.23	0.90–0.95	0.29–0.30	0.16–0.20
NGC 1292	25–48	0.22–1.53	0.05–0.30	0.06–0.24	0.04–0.21
NGC 1300	30–36	0.21–0.23	0.80–0.93	0.19–0.21	0.14–0.16
NGC 1353	6–19	1.31–21.0	0.01–0.12	0.01–0.08	0.01–0.05
NGC 1365	3–7	0.83–31.0	0.15–0.83	0.02–0.10	0.01–0.02
NGC 1964	40–48	0.27–0.42	0.40–0.52	0.30–0.35	0.21–0.23
NGC 3223	43–48	0.59–0.92	0.99–1.00	0.16–0.24	0.14–0.17
NGC 3318	32–38	0.19–0.28	0.75–0.95	0.25–0.34	0.16–0.21

NOTE. — Model results from the no-AC models.

TABLE 3
GALAXY MODEL RESULTS BY DIRECT ROTATION CURVE FITTING

Galaxy Name	c_{vir}	$M_{\text{vir}} (M_{\odot})$
ESO 009-G010	15.0	1.05×10^{12}
ESO 582-G012	39.0	2.50×10^{11}
IC 4808	47.0	3.87×10^{11}
NGC 150	48.0	2.91×10^{11}
NGC 578	47.0	9.50×10^{11}
NGC 908	47.0	2.25×10^{11}
NGC 1292	35.0	1.53×10^{12}
NGC 1300	35.0	2.33×10^{11}
NGC 1353	11.0	4.38×10^{12}
NGC 1365	7.0	8.28×10^{11}
NGC 1964	48.0	3.26×10^{11}
NGC 3223	44.0	9.15×10^{11}
NGC 3318	35.0	2.08×10^{11}

orbital time. This slow infall results in the halo density distribution contracting adiabatically, which gives rise to a more concentrated dark matter halo. AC was originally discussed as a means of producing featureless rotation curves for large disk galaxies (Rubin et al. 1985), but it has also proven accurate in describing spiral galaxy formation in N-body simulations (e.g., Gnedin et al. 2004, 2010, and references therein). Nevertheless, the degree to which AC operates in real galaxies is uncertain (see Seigar & Berrier 2011 for a review).

For our AC model, we use the prescription described by Blumenthal et al. (1986). Gnedin et al. (2004) suggest a slightly modified prescription, but the differences between the two methods are small compared to the differences between our AC model and our non-AC model. In principle, any observational probe that can distinguish between AC and non-AC-type scenarios provides an important constraint on the nature of gas infall into galaxies (i.e., was it fast or was it slow?).

For each galaxy we iterate over the central and $\pm 1\sigma$ values found in the bulge-disk decompositions for R_d and L_{disk} and explore the five values of mass-to-light ratio discussed above, $(M/L) = 0.7, 0.8, 0.9, 1.0,$ and 1.1 , assuming that M/L remains constant with radius. For each choice of bulge-disk model parameters and mass-to-light ratios, we allow the (initial) halo NFW concentration parameter to vary over the range of viable values, $c_{\text{vir}} \geq 3$ (Bullock et al. 2001b). We then determine the halo virial mass M_{vir} necessary to reproduce the value of $V_{2.2}$ for the galaxy and determine the implied fraction of the mass in the system in the form of stars compared to that “expected” from the Universal baryon fraction, $f_* = M_*/(f_b M_{\text{vir}})$. We make the demand that f_* lies within the range of plausible values $0.01 f_b < f_* < f_b$. Note that the $V_{2.2}$ is the rotation velocity (in km s^{-1}) at 2.2 disk scalelengths. We chose $V_{2.2}$ because it is where the disk contribution to the rotation curve is a maximum.

For each chosen value of c_{vir} and adopted disk galaxy formation scenario, the chosen $V_{2.2}$ constraint defines a complete rotation curve and thus provides a shear at every radius. The three panels of Figure 3 show the results of this exercise for the 13 galaxies in our sample. In each panel, open symbols are for the non-AC model, and the filled symbols are for the AC model. Each point rep-

resents a distinct input combination of R_d, L_{disk} , and M/L . The measured shear rate illustrated by a solid vertical line, and the $\pm 1\sigma$ range in the observed shear for each galaxy is shown by the two vertical dashed lines in each panel.

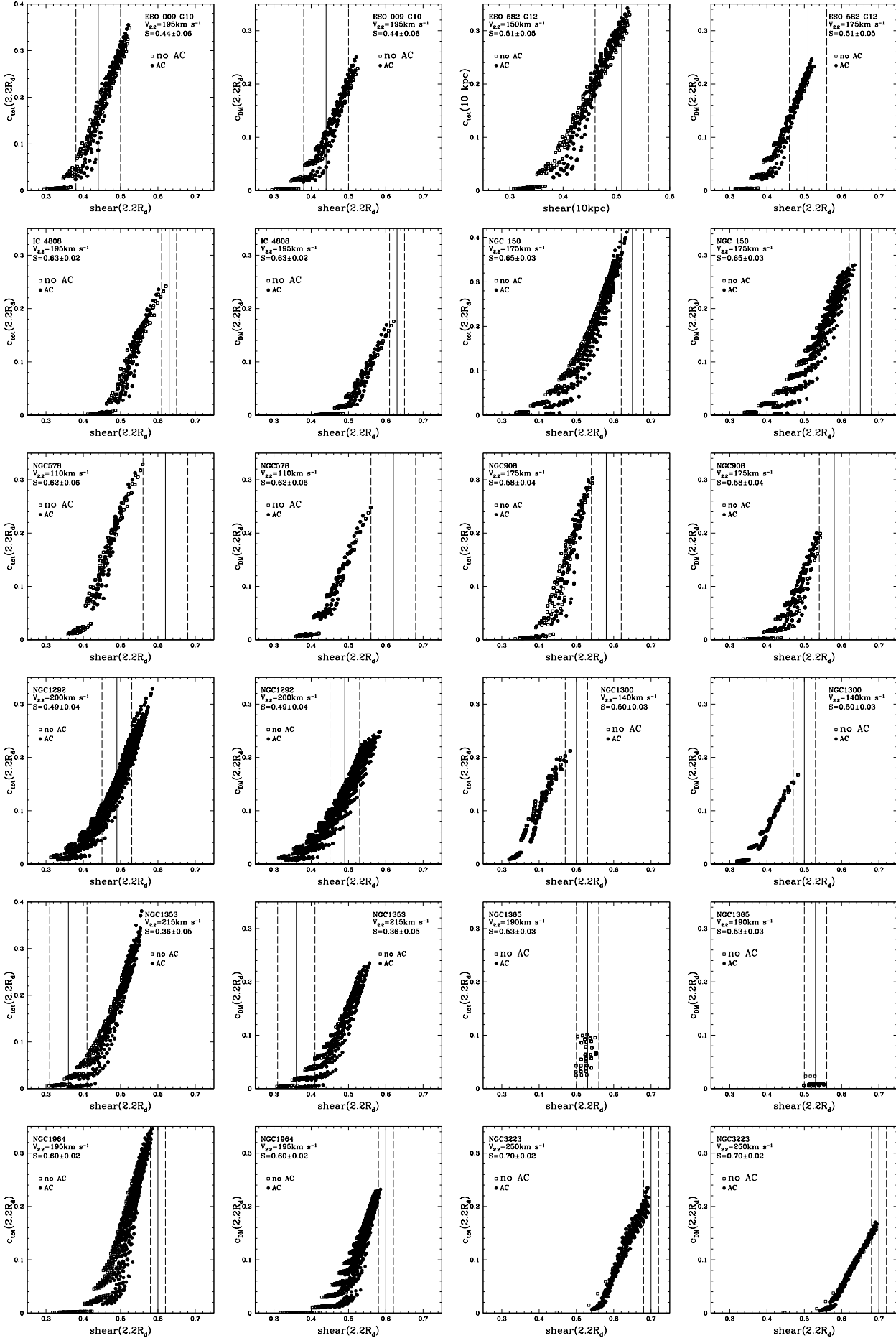
Consider first the left panel of Figure 3. Here we plot the dark matter halo concentration parameter versus the shear measured at $2.2R_d$. More concentrated halos generally produce higher shears, as expected. It can be seen that for a given NFW concentration, c_{vir} , several values of shear are possible. This is due to changes in the baryon contribution (i.e., the disk mass and disk scale length) to the rotation curve. Whether an increase in the baryon contribution causes the shear to increase or decrease depends on the size of the disk (i.e., the disk scale length). The same is true for all of our galaxies. In the AC model (filled circles), c_{vir} refers to the halo concentration before the halo is adiabatically contracted. This is why the AC points tend to have higher shear values at fixed c_{vir} compared to the non-AC case. Every point (or $R_d, L_{\text{disk}}, M/L$ input combination) has an associated dark halo virial mass M_{vir} and stellar baryon fraction f_* . These values are plotted versus shear rate in the middle and right panels in Figure 3. Observe that with only the $V_{2.2}$ constraint imposed (all points), a wide range of dark matter halo properties are allowed. Once we constrain the models by forcing the predicted shear to be consistent with the observed range, we prefer a much narrower range of halo concentrations, virial masses, and stellar baryon fractions, although favoring one type of model over another (i.e., our AC versus our non-AC model) is unfortunately difficult in most cases, if not impossible.

Model results for the central mass concentration in each galaxy are shown in Figure 4. Here c_{tot} and c_{dm} correspond to the fraction of the total and dark matter mass contained within 2.2 disk scalelengths of each galaxy. The ranges of allowed values for each of the five parameters in Figures 3 and 4 are listed in Table 2 for all of the galaxies in our sample.

5. DISCUSSION

The work presented in this paper clearly demonstrates that the shear rate adds an important constraint on galaxy formation models compared to what can be learned from standard Tully-Fisher constraints alone. In an earlier paper (Seigar et al. 2006) we showed some tantalizing results for two galaxies, IC 2522 and ESO 582-G12 (one of which we have updated the results for in this paper). With a further 12 galaxies now analyzed using the shear-pitch angle relation, we have demonstrated that this technique can be extremely useful for determining mass concentrations in galaxies, especially for statistically large samples, where the statistics of the sample outweighs any uncertainties in the derived parameters (e.g., M_{vir} and c_{vir}) for any individual galaxy.

Before we proceed to perform such an analysis (which will actually be presented in a forthcoming paper), we first proceed with a further test of the modeling presented here. Since the sample of galaxies we present here have observed $H\alpha$ rotation curves, an important test of our modeling is how well the modeled rotation curves fit the data. In this case, we take the no-AC models that describe the shear most accurately (i.e., those with a combination of R_d, L_{disk} , and M/L that accurately



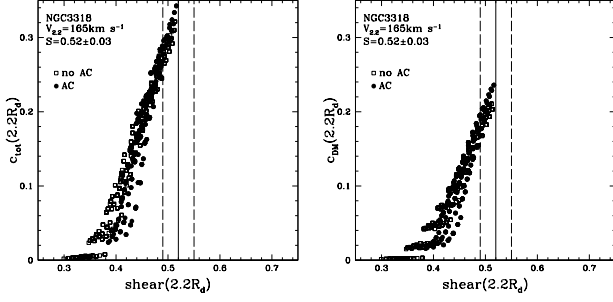


FIG. 4.— Model results for 13 galaxies. *Left*: Central mass concentration (mass fraction within $2.2R_d$) vs. shear; *right*: dark matter concentration (dark matter mass fraction within $2.2R_d$) vs. shear. The open squares represent the model without adiabatic contraction of the stellar halo, and filled circles represent the model with adiabatic contraction. The vertical lines present the measured shear (*solid line*) with the 1σ error added and subtracted (*dashed lines*).

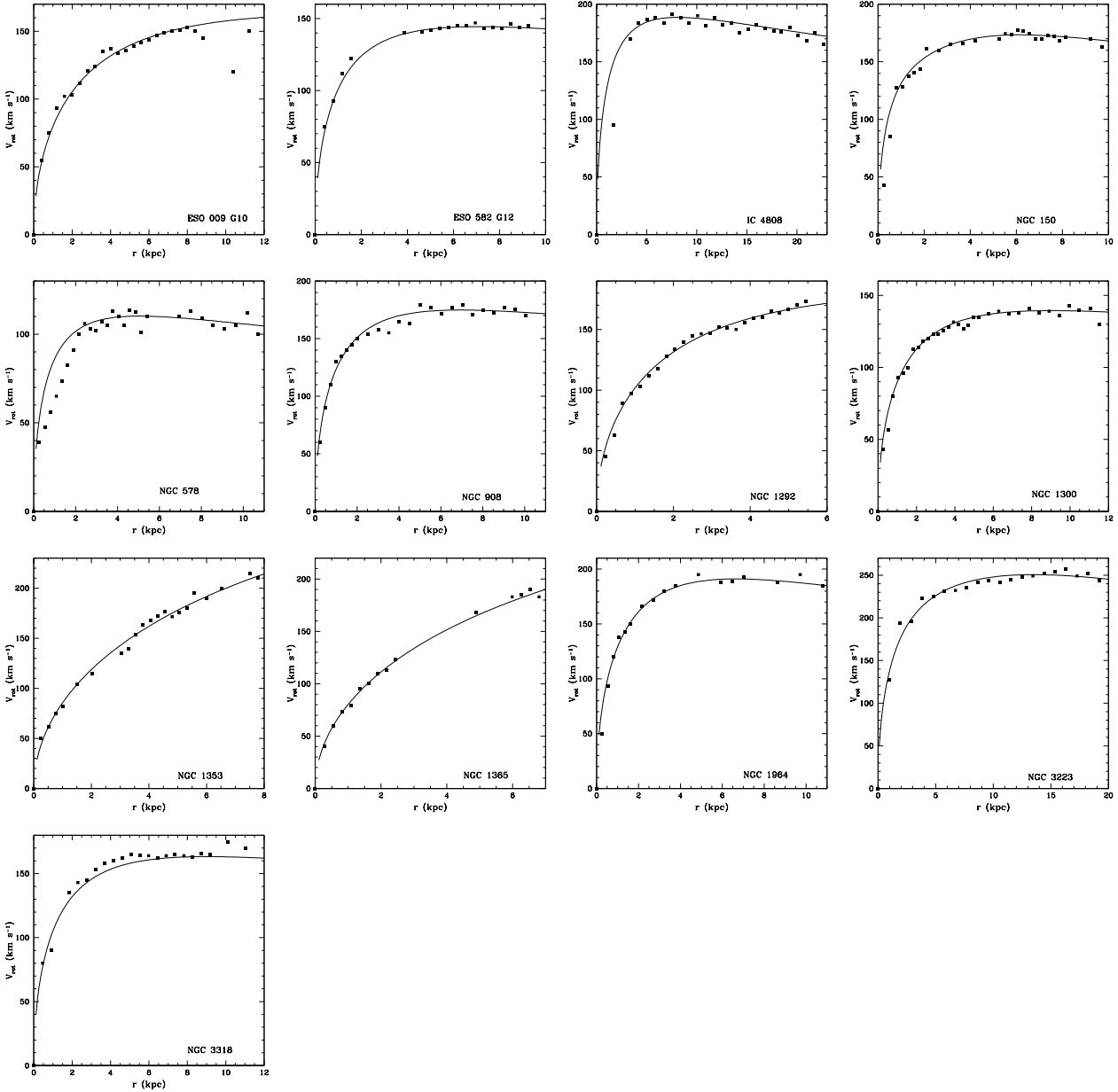


FIG. 5.— Observed rotation curves with the overlaid model rotation curves for 13 galaxies. The errors on the data points are typically $< 10\%$ (Persic & Salucci 1995). The solid lines represent the rotation curve that best matches the observed shear at $2.2R_d$.

predict the shear as determined from Figures 3 and 4), and find which model best fits the observed $H\alpha$ rotation curves from Persic & Salucci (1995). We have chosen to work with only our no-AC models here as we could not rule out one type of model over the other (i.e., AC model versus no-AC model), and for consistency we chose the pure NFW model here (i.e., the no-AC model). Furthermore, several papers (e.g., Kassin et al. 2008a, b) have shown that AC rarely operates, and that rotation curves can be described without the need for AC. Nevertheless some examples (e.g., M31) have been shown to require AC (e.g., Klypin et al. 2002; Seigar et al. 2008a). The virial mass and NFW concentrations resulting from this are listed in Table 3.

The results of our model fits to the observed data are presented in Figure 5, which shows the Persic & Salucci (1995) $H\alpha$ rotation overlaid with our modeled rotation curves. In all cases the rotation curve is modeled well in the outer parts, where we are measuring the shear. Furthermore, in all but one case (NGC 578), the inner parts of the rotation curve are modeled extremely well.

Given the further constraints placed on the NFW concentration parameter (c_{vir}) by finding the model that best fits the observed rotation curve (figure 5), we can now compare this parameter with other properties of the galaxy. Recent results have suggested that there may be a link between the mass of supermassive black holes (SMBHs) in galaxy nuclei and the dark halo concentration parameter. For example, Booth & Schaye (2009) explored a potential connection between SMBH mass and dark matter halos using a series of simulations. Treuthardt et al. (2012) developed this further using a combination of imaging data and simulated galaxies, but could not come to any strong conclusions due to a lack of dynamical information. Furthermore, observations of AGN (active galactic nuclei) in galaxies with little or no bulge, suggest that the dark matter halo concentration may play a role in the determination of SMBH mass (Satyapal et al. 2007, 2008). These arguments have been used to explain the recent discovery of a correlation between SMBH mass and spiral arm pitch angle in disk galaxies (Seigar et al. 2008b; Berrier et al. 2012). If the fundamental factor in determining SMBH mass is dark matter halo concentration (e.g., Ferrarese 2002; Satyapal et al. 2007, 2008), then all of the observed relationships naturally follow. Nevertheless it is important to point out that Kormendy & Bender (2011) have provided arguments that suggest that the dark matter concentration does not have any direct correlation with the properties of the SMBH. However, their paper did not take into account the theoretical work of Booth & Schaye (2009), which suggests that the SMBH growth is regulated by the dark matter halo concentration. Shortly after the publication of Kormendy & Bender (2011) further observational constraints provided evidence that the SMBH mass is correlated with properties of the dark matter halo (Volonteri et al. 2011).

Given the apparent controversy over the link between SMBH mass and dark matter concentration, we realized that the parameters we had derived could be used to shed some light on this question. Using the concentration parameters derived by fitting our models directly to the observed rotation curves, we tested the correlation between NFW concentration (c_{vir}) and the spiral arm

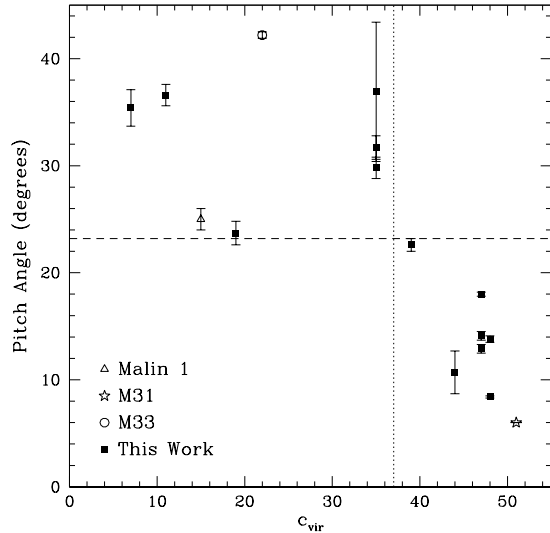


FIG. 6.— Spiral arm pitch angle vs. NFW concentration. The open triangle represents Malin 1 (Seigar 2008), the star represents M31 (Seigar et al. 2008), the open circle represents M33 (Seigar 2011) and the filled squares represent the current sample.

pitch angles of these galaxies, using the fact that pitch angle can be used as a proxy for SMBH mass (Seigar et al. 2008b; Berrier et al. 2012). The result can be seen in Figure 6.

Note that the NFW concentrations here are derived from our no-AC models, as described in the direct rotation curve fitting above in section 4. Figure 6 also includes data for M31 (Seigar et al. 2008), M33 (Seigar 2011), and Malin 1 (Seigar 2008). Although these authors report that an AC model works best for Malin 1 and M31, for consistency, here we use the concentration parameter for the no-AC model that they used. In the case of M33, the authors only report a pure NFW concentration.

Figure 6 does not show a strong correlation between spiral arm pitch angle (or SMBH mass) and the NFW concentration parameter. However, there does appear to be a trend whereby galaxies with very open spirals (i.e., with a pitch angle, $P > 23^\circ$) seem to have lower concentrations than those with tightly wound spirals (with $P < 23^\circ$). There is a word of caution however. The cutoff for the concentration parameter corresponding to this pitch angle is $c_{\text{vir}} \simeq 37$. For the eight galaxies with $P < 23^\circ$, the concentration is in the range $37 \leq c_{\text{vir}} \leq 51$. These are extremely high concentrations. This range corresponds to a $\sim 3\sigma$ – $\sim 4.4\sigma$ outliers from the expected concentration distribution for large spiral galaxies (e.g., Bullock et al. 2001a). Indeed, high concentrations such as these have been used as an argument against a pure NFW dark matter density profile, and instead it has been suggested that in these cases, an adiabatically contracted profile should be adopted (see for example the case of M31 in Seigar et al. 2008a). Indeed, if we chose to adopt our AC models in these cases (i.e., for tight spirals or high concentrations), Figure 3 shows that there is a tendency for the NFW concentration to decrease. One should note that this is the initial NFW concentration, but it is in better agreement with the expected distribution of c_{vir} as given by Bullock et al. (2001a), although the halo does

become more concentrated due to AC.

6. SUMMARY AND CONCLUDING REMARKS

In this paper we have examined *Spitzer IRAC* 3.6- μm images of 13 galaxies that have $\text{H}\alpha$ rotation curves in the literature. Using these galaxies we have shown that:

- The relation between spiral arm pitch angle and rotation curve shear still exists, although with a slightly larger scatter than had been presented in Seigar et al. (2006).
- Using shear (or pitch angle as a proxy for shear) as well as a maximum rotation velocity (or galaxy luminosity as a proxy) we can constrain various parameters related to the dark matter halo (e.g., virial mass, NFW concentration, etc.) and parameters relating to the total mass concentration of these galaxies.
- There appears to be a weak trend between spiral arm pitch angle and NFW concentration parameter, whereby galaxies with tightly wound arms (i.e., $P < 23^\circ$) have particularly high concentrations. For these galaxies we suggest that AC may play a role, which would help to bring their dark matter concentrations down into a range that is more consistent with dark matter halo simulations for spiral galaxies.

It should be noted that the role of the baryon-dominated central spheroidal component (i.e., the bulge) has remain untouched in this paper. However, we have shown that we can derive useful dynamical information from imaging data alone (we can get a maximum rotation velocity from the galaxy luminosity, and we can get the slope of the rotation curve — or shear — from a spiral arm pitch angle) and in future papers we intend to apply

this method to a much larger sample of galaxies. Some forthcoming projects we have in mind are as follows:

- In a recent paper by Davis et al. (2014), we defined a volume-limited sample of Southern Hemisphere spiral galaxies with a limiting absolute B band magnitude of $M_B = -19.528$ and a redshift limit of $z = 0.0068$. We now intend to measure the 3.6- μm spiral arm pitch angles of these galaxies, and determine their mass concentrations using the methods described here. We will also investigate whether choosing one exponential scalelength, R_d , rather than $2.2R_d$ for the radius at which shear is measured, significantly affects the best-fitting dark matter halo concentrations (c_{vir}) and virial masses (M_{vir}). This may give us some handle on the affect of the bulge component, and therefore tell us something about whether the pitch angles and SMBH masses depend on c_{vir} or a combination of c_{vir} and the bulge mass. This work will be published in Paper 3 of this series.
- A fourth (and final) paper in this series will measure spiral arm pitch angles of disk galaxies in the GOODS-S and -N fields. This will result in a determination of mass concentrations in galaxies as a function of lookback time.

This research has made use of the NASA/IPAC Extragalactic Database (NED) which is operated by the Jet Propulsion Laboratory, California Institute of Technology, under contract with the National Aeronautics and Space Administration. The authors wish to thank Paolo Salucci for supplying the rotation curve data from which shear and the $V_{2.2}$ velocities were derived for some of the galaxies in this paper. We also thank the referee whose comments improved the content of this paper.

REFERENCES

- Bell, E. F., McIntosh, D. H., Katz, N., & Weinberg, M. D. 2003, *ApJS*, 149, 289
- Berrier, J. C., Davis, B. L., Kenefick, D., Seigar, M. S., Hartley, M., Kenefick, J., Lacy, C. H. S., Barrows, R. S., & Bentz, M. 2012, *ApJ*, 769, 132
- Bertin, G., Lin, C. C., Lowe, S. A., & Thurstans, R. P. 1989a, *ApJ*, 338, 78
- Bertin, G., Lin, C. C., Lowe, S. A., & Thurstans, R. P. 1989b, *ApJ*, 338, 104
- Bertin, G. 1991, in *Proc. IAU Symp 146, Dynamics of Galaxies and Their Molecular Cloud Distributions*, ed. F. Combes, & F. Casoli (Dordrecht: Kluwer), 93
- Bertin G. 1993, *PASP*, 105, 640
- Bertin G. 1996, In *New Extragalactic Perspectives in the New South Africa*, ed. D. L. Block, & J. M. Greenberg (Dordrecht: Kluwer), 227
- Bertin G., & Lin C. C. 1996, *Spiral Structure in Galaxies: A density wave theory* (Cambridge: MIT Press)
- Block, D. L., Puerari, I., Frogel, J. A., Eskridge, P. B., Stockton, A., & Fuchs, B. 1999 *Ap&SS*, 269, 5
- Blumenthal, G. R., Faber, S. M., Flores, R., & Primack, J. R. 1986, *ApJ*, 301, 27
- Booth, C. M., & Schaye, J. 2009, *MNRAS*, 398, 53
- Bullock, J. S., Dekel, A., Kolatt, T. S., Kravtsov, A. V., Klypin, A. A., Porciani, C., & Primack, J. R. 2001a, *ApJ*, 555, 240
- Bullock, J. S., Kolatt, T. S., Sigad, Y., Somerville, R. S., Kravtsov, A. V., Klypin, A. A., Primack, J. R., & Dekel, A. 2001b, *MNRAS*, 321, 559
- Capaccioli M., 1987, in *IAU Symp. 127, Structure and Dynamics of Elliptical Galaxies*, ed. P. T. de Zeeuw (Dordrecht: Reidel), 47
- Considère, S., & Athanassoula, E. 1988, *A&AS*, 76, 365
- Davis, B. L., Berrier, J. C., Shields, D. W., Kenefick, J., Kenefick, D., Seigar, M. S., Lacy, C. H. S., & Puerari, I. 2012, *ApJS*, 199, 33
- Davis, B. L., Berrier, J. C., Johns, L., Shields, D. W., Hartley, M. T., Kenefick, D., Kenefick, J., & Seigar, M. S., Lacy, C. H. S. 2014, *ApJ*, 749, 124
- de Jong, R. S. 1996, *A&A*, 313, 45
- de Vaucouleurs G., 1948, *AnAp*, 11, 247
- de Vaucouleurs G., 1957, *AJ*, 62, 69
- de Vaucouleurs, G., de Vaucouleurs, A., Corwin, H. G., Jr., Buta, R. J., Paturel, G., & Fouqué, R. 1991, *The Third Reference Catalog of Bright Galaxies*, (New York: Springer) (RC3)
- Fall, S. M., & Efstathiou, G. 1980, *MNRAS*, 193, 189
- Ferrarese, L. 2002, *ApJ*, 578, 90
- Fuchs, B. 1991, in *Dynamics of Disk Galaxies*, ed. B. Sundelius (Göteborg: Chalmers Univ. of Technology), 359
- Fuchs, B. 2000, in *ASP Conf. Ser. 197, Dynamics of Galaxies: from the early universe to the present*, ed. F. Combes, G. A. Mamon, & V. Charmandaris, (San Francisco: ASP), 53
- Gnedin, O. Y., Kravtsov, A. V., Klypin, A. A., & Nagai, D. 2004, *ApJ*, 616, 16
- Gnedin, O. Y., Brown, W. R., Geller, M. J., & Kenyon, S. J. 2010, *ApJ*, 720, L108
- Graham A. W., Driver S. P., 2005, *PASA*, 22, 118

- Ho, L. C., Li, Z. Y., Barth, A. J., Seigar, M. S., & Peng, C. Y. 2011, *ApJS*, 197, 21
- Jedrzejewski, R. I. 1987, *MNRAS*, 226, 747
- Kassin, S. A., de Jong, R. S., & Pogge, R. W. 2006a, *ApJS*, 162, 80
- Kassin, S. A., de Jong, R. S., & Weiner, B. J. 2006b, *ApJ*, 643, 804
- Klypin, A. A., Zhao, H., & Somerville, R. S. 2002, *ApJ*, 573, 597
- Komatsu, E. et al. 2009, *ApJS*, 180, 330
- Kormendy, J., & Bender, R. 2011, *Nature*, 469, 377
- Navarro, J. F., Frenk, C. S., & White, S. D. M. 1997, *ApJ*, 462, 563 (NFW)
- Persic, M., & Salucci, P. 1995, *ApJS*, 99, 501
- Pizagno, J., et al. 2005, *ApJ*, 633, 844
- Satyapal, S., Vegam D., Heckman, T., O'Halloram, B., & Dudik, R. 2007, *ApJ*, 663, L9
- Satyapal, S., Vega, D., Dudik, R. P., Abel, N. P., & Heckman, T. 2008, *ApJ*, 677, 926
- Schröder, M. F. S., Pastoriza, M. G., Kepler, S. O., & Puerari, I. 1994, *A&AS*, 108, 41
- Seigar, M. S. 2005, *MNRAS*, 361, L20
- Seigar, M. S., & James, P. A. 1998a, *MNRAS*, 299, 672
- Seigar, M. S., & James, P. A. 1998b, *MNRAS*, 299, 685
- Seigar, M. S., Block, D. L., & Puerari, I. 2004, in *Penetrating Bars Through Masks of Cosmic Dust: The Hubble Tuning Fork Strikes a New Note*, ed. D. L. Block, I. Puerari, K. C. Freeman, R. Groess, & E. K. Block (Dordrecht: Springer), 155
- Seigar, M. S., Block, D. L., Puerari, I., Chorney, N. E., & James, P. A. 2005, *MNRAS*, 359, 1065
- Seigar, M. S., Bullock, J. S., Barth, A. J., & Ho, L. C. 2006, *ApJ*, 645, 1021
- Seigar, M. S. 2008, *PASP*, 120, 945
- Seigar, M. S., Barth, A. J., & Bullock, J. A. 2008a, *MNRAS*, 389, 1911
- Seigar, M. S., Kennefick, D., Kennefick, J., Lacy, C. H. S. 2008b, *ApJ*, 678, L93
- Seigar, M. S. 2011, *ISRAA*, 2011, 725697
- Seigar, M. S., & Berrier, J. 2011, in *Advances in Modern Cosmology*, ed. A. Ghribi, InTech Publications (Croatia)
- Treuthardt, P., Seigar, M. S., Sierra, A. D., Al-Baidhany, I., Salo, H., Kennefick, D., Kennefick, J., & Lacy, C. H. S. 2012, *MNRAS*, 423, 3118
- Tully, R. B., & Fisher, J.R. 1977, *A&A*, 54, 661
- Volonteri, M., Natarajan, P., & Gültekin, K. 2011, *ApJ*, 737, 50